Resolving the nature of the Rosette HH1 jet facing strong UV dissipation

Jin Zeng Li[1], You-Hua Chu[2,3], Robert A. Gruendl[2], John Bally[4,5] and Wei Su[1]

ABSTRACT

The Rosette HH1 jet is a collimated flow immersed in the strong UV radiation field of the Rosette Nebula. We investigate the physical properties of the Rosette HH1 jet using high-quality narrow-band images and high-dispersion spectroscopy. The new images show that the axis of the jet is not precisely aligned with the star near the base of the jet. The high resolution of the spectra allows us to accurately determine the contributions from the H II region, jet, and star. The appoaching and receding sides of the expanding shell of the Rosette Nebula are at heliocentric velocities of 13 and 40 km s^{-1}, while the jet reaches a maximum velocity offset at a heliocentric velocity of -30 km s^{-1}. The [S II] doublet ratios indicate an electron density of $\sim$1000 cm^{-3} in the jet and $\leq$100 cm^{-3} in the H II region. With a careful subtraction of the nebular and jet components, we find the stellar Hα line is dominated by a broad absorption profile with little or no emission component, indicating a lack of substantial circumstellar material. The circumstellar material has most likely been photo-evaporated by the strong UV radiation field in the Rosette Nebula. The evaporation time scale is 10^3 – 10^4 yr. The Rosette HH1 jet source provides evidence for an accelerated evolution from a CTTS to a WTTS due to the strong UV radiation field; therefore, both CTTSs and WTTSs can be spatially mixed in regions with massive star formation.

Subject headings: accretion, accretion disks — ISM: Herbig-Haro objects — ISM: jets and outflows — stars: formation — stars: pre-main sequence

[1]National Astronomical Observatories, Chinese Academy of Sciences, Beijing 100012, China; ljz@bao.ac.cn

[2]Department of Astronomy, University of Illinois, Urbana-Champaign, IL, 61801

[3]Visiting Astronomer, Cerro Tololo Inter-American Observatory

[4]Center for Astrophysics and Space Astronomy, and Department of Astrophysical and Planetary Sciences, University of Colorado, Campus Box 389, Boulder, CO 80309-0389

[5]Visiting Astronomer, Kitt Peak National Observatory

1. Introduction

Herbig-Haro (HH) objects immersed in an ultraviolet (UV) radiation field can be photoionized externally (Reipurth et al. 1998). The photoionized jets/outflows of HH objects become optically visible, and thus their detailed physical properties can be studied. Such photoionized HH jet systems have been identified in the Orion Nebula and in the reflection nebula NGC 1333 (Bally et al. 2000; Bally & Reipurth 2001). Recently, two such photoionized jet systems, the Rosette HH1 and HH2 jets, were discovered within the central cavity of the Rosette Nebula (Li 2003; Li & Rector 2004). The Rosette Nebula is a spectacular H II region excavated by strong stellar winds from dozens of OB stars at the center of the young open cluster NGC 2244, the primary component of a possible twin cluster recently identified using the 2MASS (Two Micron All Sky Survey) database (Li 2005). At a distance of ~ 1.39 kpc (Hensberge, Pavlovski, & Verschueren 2000), this emerging young open cluster is found to have a main sequence turn-off age of about 1.9 Myr (Park & Sung 2002).

The photoionized jets discovered in the Rosette Nebula (Li 2003; Li & Rector 2004) and their counterparts found in the vicinity of σ Orionis (Reipurth et al. 1998) are both bathed in harsh UV radiation from massive OB stars within a few parsecs, and thus share many similar properties consistent with an irradiated origin of the jet systems: (1) Their jet-driving sources are visible and show spectral characteristics of T Tauri stars. (2) These sources were not detected by *IRAS* (*Infrared Astronomical Satellite*), indicating a lack of circumstellar material such as extended disks and/or envelopes. (3) The jets show [S II]/Hα line ratio decreasing from the base outward, indicating that the dominant excitation mechanism changes from shocks at the base to photoionization at the end of the jet. (4) The jet systems all have a highly asymmetric or even unipolar morphology, indicating perhaps different jet forming conditions in the launch and collimation regions.

The Rosette HH jets show subtle differences from other externally photoionized HH jets because of different degrees of hardness in the UV radiation field or strength of fast stellar winds. Both the Rosette HH1 and HH2 jets show high excitation (Li & Rector 2004), as the Rosette Nebula contains an O4 star and an O5 star (Pérez et al. 1987). In the Orion Nebula, HH jets with [O III] emission are found only within $30''$, or $\sim$0.06 pc, from θ^1 Ori C, an O4-6 star, the earliest O star in the Orion Nebula (Maíz-Apellániz et al. 2004). The high excitation of these HH jets results from both the harsh UV radiation and strong fast stellar wind of θ^1 Ori C (Bally et al. 1998).

Li & Rector (2004) propose that the Rosette jets provide evidence for efficient dissipation of circumstellar disks and envelopes in the close vicinity of massive OB stars. This UV dissipation of pre-existing protostellar systems may lead to the formation of isolated brown dwarfs (BDs) and free-floating giant planets. Such a formation mechanism

for single sub-stellar objects has indeed been shown to be effective by theoretical studies (Whitworth & Zinnecker 2004).

It is therefore important to explore the nature of jet formation and disk dissipation of low-mass YSOs in close vicinity of massive ionizing OB stars, as the occurrence of such OB clusters and associations is common in the Galaxy, and the solar system may have been formed in such environments (Looney, Tobin, & Fields 2006). Furthermore, there has been an on-going debate whether weak-lined T Tauri stars (WTTSs) evolve from classical T Tauri stars (CTTSs) through gradual dissipation of circumstellar material, or WTTSs are formed through rapid disk dissipation due to external forces after the formation of the protostar. A detailed study of the Rosette jet systems may provide insight on the rapid evolution of CTTSs to WTTSs due to external photoionization of their protostellar disks in massive star forming regions. WTTSs formed in this way have indistinguishable evolutionary ages from those of CTTS that originated from the same episode of star formation.

Meaburn et al. (2005) presented a kinematical study of the Rosette HH1 jet and confirmed the jet nature of the system. Here we investigate in detail the physical nature of the jet system using high-resolution imaging and echelle spectroscopy, as well as data from a simultaneous photometric and spectroscopic monitoring of the jet-driving source.

2. Observations and Data Reduction

2.1. Narrow-band Imaging

Narrow-band Hα images of the Rosette Nebula were obtained with the 8k×8k MOSAIC CCD camera on the Mayall 4 m telescope at the Kitt Peak National Observatory on 2001 October 13. A set of five 600 s exposures was taken, with each image slightly offset to fill in physical gaps between the MOSAIC CCDs. The pixel scale is $0\farcs258$ pixel^{-1}, resulting in roughly a $36' \times 36'$ field of view.

2.2. Echelle Spectroscopy

We obtained high-dispersion spectroscopic observations of Rosette HH 1 with the echelle spectrograph on the Blanco 4 m telescope at the Cerro Tololo Inter-American Observatory on 2004 January 9 and 12. In each observation a 79 line mm^{-1} echelle grating was used. The observations on 2004 January 9 were made in a multi-order mode, using a 226 line mm^{-1} cross-disperser and a broad-band blocking filter (GG385). The spectral coverage is roughly

4000–7000 Å, so that nebular lines of a range of excitation can be examined. In the case of the [S II] $\lambda\lambda$6717, 6731 doublet, the line ratio has been used to estimate the electron densities within the jet. The observations on 2004 January 12 were made in a single-order mode, using a flat mirror and a broad Hα filter (central wavelength 6563 Å with 75 Å FWHM) to isolate the order containing the Hα and [N II] $\lambda\lambda$6548, 6583 lines. The exposure time used for both instrumental setups was 1,200 s.

For each observation the long-focus red camera was used to obtain a reciprocal dispersion of 3.5 Å mm^{-1} at Hα. The spectra were imaged using the SITe2K #6 CCD detector. The 24 μm pixel size corresponds to $0\farcs26$ pixel^{-1} along the slit and $\sim$0.08 Å pixel^{-1} along the dispersion axis. Both observations used a $1\farcs6$ slit oriented roughly along the jet direction, at position angles of 312° (multi-order) and 318° (single-order). The resultant instrumental resolution, as measured by the FWHM of the unresolved telluric emission lines, was 0.29 Å or 13 km s^{-1} at Hα.

The observations were reduced following standard procedures in the IRAF (Ver. 2.12) software package. This included bias correction, flat-fielding and gain-jump removal between the chips. Cosmic-ray hits were manually rejected from the 2D spectrograms. Wavelength calibration of the data was carried out based on Th-Ar lamp exposures and further improved by comparison with night sky emission lines, which resulted in an accuracy of $\sim$1 km s^{-1} before converting to the heliocentric frame.

2.3. Simultaneous Photometric and Spectroscopic Monitoring

We have carried out a simultaneous photometric and spectroscopic monitoring campaign of the Rosette HH1 source between 2004 December 31 and 2005 January 7. The time-series photometric observations, unaccompanied by spectroscopy, were further extended from January 8 to January 13. The photometric observations were made in B and R filters with the 0.8 m telescope of the Hsing-Hua University, located at the Xing-Long station of the National Astronomical Observatory of the Chinese Academy of Sciences (NAOC). Differential photometry of the jet-driving source was obtained through comparisons with two slightly brighter stars in the same field at α(J2000) = $06^{\rm h}32^{\rm m}15\fs47$, δ(J2000) = $04°55'20\farcs27$ and α(J2000) = $06^{\rm h}32^{\rm m}22\fs69$, δ(J2000) = $04°54'05\farcs31$. The R band photometry of the reference stars is found to be constant within 0.04 mag throughout the monitoring campaign. Many of the B band exposures were affected by charge bleeding from the saturated O9.5 star HD 46241. These unreliable data are not presented here.

Low-resolution spectroscopy of the jet source was obtained with the 2.16 m telescope

of NAOC during this monitoring campaign. Two different spectrographs were used. From 2004 December 31 to 2005 January 4, the Beijing Faint Object Spectrograph and Camera (BFOSC), a copy of EFOSC in service at the European Southern Observatory, and a thinned back-illuminated Orbit 2k × 2k CCD were used. The G4 grating was employed, which gave a two-pixel resolution of 8.3 Å. On 2005 January 5–7, an OMR (Optomechanics Research Inc.) spectrograph and a Tecktronix 1024 × 1024 CCD were used. These spectroscopic data have a higher resolution, with a 100 Å mm^{-1} reciprocal dispersion and a two-pixel resolution of 4.8 Å. Both sets of observations used a 2″ slit. The spectroscopic data were reduced using standard procedures and packages in IRAF. The CCD reductions included bias and flat-field correction, nebular background subtraction, and cosmic rays removal. Wavelength calibration was performed using He-Ar lamp exposures at both the beginning and the end of the observations every night. Flux calibration of each spectrum was based on observations of at least 2 of the KPNO spectral standards (Massey et al. 1988) per night.

3. Morphology and Kinematics of the Jet

Figure 1 presents our new Hα image of the Rosette HH1 jet. This high-quality image reveals that the jet does not trace back through the exact center of the jet-driving source. The morphology of the jet appears to indicate episodic or nonsteady mass ejection. A close inspection shows a split at the end of the collimated jet, with one branch remaining straight while the other bending north possibly as a result of an interaction with the stellar wind of the O4 star, HD 46223.

In Figure 2, we present the echelle spectrograms of the Rosette HH1 jet. The continuum emission at the origin of each spectrogram is from the jet-driving source. The single-order observations cover only the Hα and [N II] lines (the two panels to the left in Fig. 2). The multi-order observations detected the Hα, Hβ, Hγ, He I λ5876, [N II] $\lambda\lambda$6548, 6583, [O III] $\lambda\lambda$4959, 5007, and [S II] $\lambda\lambda$6716, 6731 lines. The three panels to the right in Figure 2 show the [N II] λ6583, [S II] λ6731, and [O III] λ5007 lines (the brighter component of each doublet). These lines have different thermal widths and require different excitation energies, and thus appear different and can be intercompared to gain physical insight.

The [N II] lines have smaller thermal widths than the Hα line and thus resolve the velocity structures of the HH jet and the superposed nebula more clearly. The [N II] lines detect a prominent irregular component at the location of the jet. This jet component is blue-shifted with respect to two nebular components that have nearly uniform velocity and surface brightness throughout the slit. These two nebular components, at heliocentric velocities ($V_{\rm hel}$) of ∼13 and 40 km s^{-1}, arise from the approaching and receding sides of the

Rosette Nebula's expanding shell. These velocities imply a systemic velocity of $V_{\rm hel} \sim 27$ km s^{-1} and an expansion velocity of $\sim$14 km s^{-1}. The extreme velocity of the jet reaches $V_{\rm hel} = -30$ km s^{-1}, which is blue-shifted from the Rosette's sytemic velocity by 57 km s^{-1}. These results are consistent with those reported by Meaburn et al. (2005).

In the single-order observation along PA = 318°, the [N II] emission of the jet shows two bright knots and two faint knots, with the outermost knot being the faintest. No emission from a counterjet is detected. The multi-order observation has a shorter slit along a slightly different position angle, PA = 312°, and thus shows a slighly different velocity structure in the [N II] line. The [S II] emission shows velocity structure and surface brightness similar to those of the [N II] emission. The [O III] emission, on the other hand, shows a smooth surface brightness distribution, in contrast to the knots seen in the other lines.

The observed velocity FWHM of the [N II] line ranges from $\sim$16 to $\sim$23 km s^{-1}, with the fainter knots showing broader velocity widths. These widths are not much larger than the observed FWHM of 18-20 km s^{-1} in the Rosette expanding shell components. For an instrumental FWHM of 12 km s^{-1} and a thermal width of 5.7 km s^{-1} for [N II] at 10^4 K, the observed FWHM of the jet implies an intrinsic turbulent FWHM of 9 to 19 km s^{-1}.

4. Stellar Hα Profile

One interesting spectral feature suggested by Li & Rector (2004) for the jet-driving source is an inverse P Cygni profile at the Hα line based on a low-dispersion spectrum. An inverse P Cygni profile, if confirmed, indicates that material is being accreted onto the star. Our new high-dispersion echelle observations clearly resolve both spatially and spectrally the nebular and stellar components of the Hα line profile, and thus allow a critical assessment of this suggested inverse P Cygni profile. As seen in Figure 2 and shown below, the bright nebular emission from the Rosette Nebula makes it difficult to accurately extract a clean stellar spectrum.

The nebular spectrum varies along the slit. To assess the nebular contribution, we have extracted seven Hα line profiles using 1″-wide windows and 0.″5 intervals stepping across the stellar spectrum. These Hα profiles are shown in Figure 3. The spectrum J is extracted from the jet side of the star, and the blue-shifted jet component is clearly seen. Seeing spreads the jet emission into the stellar spectra S1–S4. The contribution from the Rosette Nebula is better represented by the spectra N1 and N2, extracted outside the star on the side opposite to the jet. The average of these nebular spectra is subtracted from the four stellar spectra S1–S4. The nebula-subtracted stellar spectra S1′–S4′, displayed in Figure 4, show a narrow,

blue-shifted emission component and a broad, red-shifted absorption component superposed on a continuum.

To determine the origin of the blue-shifted emission component, we use the [N II] λ6583 forbidden line that is expected only from low-density gas, such as the Rosette Nebula and the HH1 jet. The seven [N II] line profiles extracted in a similar manner are displayed in the right panel of Figure 3, and they indeed show the two components from the Rosette Nebula throughout the slit. The [N II] profiles in the four nebula-subtracted stellar spectra, displayed in the right panel of Figure 4, show that the nebula-subtraction satisfactorily removes the emission from the Rosette Nebula and that the remaining [N II] emission is from the HH1 jet. The comparison between the nebula-subtracted Hα and [N II] profiles suggests that the blue-shifted Hα emission in the stellar spectra predominantly arises from the jet.

To obtain a clean stellar spectrum, we scale and subtract the nebula-subtracted jet spectrum (J′) from the nebula-subtracted stellar spectra (S1′–S4′) by trial and error until the [N II] emission is minimized. To better show the stellar continuum, the spectra from each step of this procedure are shown in Figure 5 over a larger wavelength range. The final clean stellar spectra S2″ and S3″ show Hα absorption with little or no blue-shifted emission. The lack of strong stellar Hα emission implies the absence of a significant disk, making it difficult to be associated with a jet. This will be discussed further in Section 7.

Our final clean stellar Hα line profile is quite different from the previously reported inverse P-Cygni profile (Li & Rector 2004). As we have illustrated above, the Hα emission is dominated by contributions from the Rosette Nebula and the HH1 jet. These emission components can be resolved and subtracted accurately only if high-dispersion spectra are used. The apparent difference between the final clean stellar Hα profiles S2″ and S3″ probably results from imperfect subtraction of the jet component, as the [N II]/Hα ratio may vary along the jet. The previously reported inverse P-Cygni profile is most likely an artifact caused by difficulties in subtracting the nebular background and jet contribution using low-dispersion spectra.

5. Photoionization and Physical Parameters of the Jet

The UV radiation in the Rosette Nebula is predominantly provided by the massive stars HD 46223 and HD 46150. HD 46223, of spectral type O4V(f), is the hottest star in NGC 2244, and produces Lyman photons at a rate of $10^{49.9}$ s^{-1} (Panagia 1973). It is located at 277″, or 2.0 pc for a distance of 1.5 kpc (Dorland & Montmerle 1987), from the HH1 jet source. HD 46150 is an O5V star projected at 433″, or 3.1 pc, from the jet source. It

produces ionizing photons at a rate of $10^{49.7}$ s^{-1} (Panagia 1973). The combined Lyman continuum emission from these two exciting stars renders 1-2 orders of magnitudes higher impact on the Rosette HH1 jet than that on similar jets discovered in the vicinity of σ Orionis (Reipurth et al. 1998) and the Trapezium stars (Bally et al. 2000). The Rosette Nebula is therefore among the most extreme environments in which photoionized jets are found. Although immersed in a photoionized medium, the presence of highly collimated jets strongly suggests the existence of at least a relic disk as a sustained feed to the surviving jet. In the case of the Rosette HH1 jet, we expect a photoevaporating disk with a configuration resembling that of HH527 in the Orion Nebula, as resolved by the *Hubble Space Telescope* (Bally et al. 2000). This could serve as a schematic impression of the appearance of the disk-jet system. Their configuration of the disk subject to photoevaporation induced dissipation is believed to be similar, although the jet associated with HH527 may be oriented at a different direction with respect to the incident UV radiation and has a low excitation, being located in the outskirts of the Orion Nebula.

The electron density of the HH1 jet was derived from the [S II] doublet ratios of $\lambda6716/\lambda6731$ measured with our multi-order echelle observation along the jet. The $\lambda6716/\lambda6731$ ratios are 0.85±0.1 in the jet and 1.3±0.1 in the Rosette Nebula. The corresponding electron densities are ∼1000 cm^{-3} in the jet and ≤100 cm^{-3} in the backgound H II region. If the HH1 jet is indeed within the cavity of the Rosette Nebula, the medium between the ionizing stars and the HH1 jet is hot and ionized with a density of ∼0.1 H-atom cm^{-3} (Townsley et al. 2003). The stellar ionizing flux at the HH1 jet would be nearly unattenuated, at a level of 2.3×10^{11} photons cm^{-2} s^{-1}. For a medium of 1000 cm^{-3} density, this flux can ionize gas to a thickness of 0.37 pc. The width of the HH1 jet (measured from Fig. 1) is $\ll 1.5''$, or $\ll$ 0.01 pc; thus the HH1 jet can be fully photoionized by the radiation from HD 46223 and HD 46150.

Using the Hα surface brightness of the HH1 jet, 3.5×10^{-5} ergs s^{-1} cm^{-2} sr^{-1}, and a density of 1000 cm^{-3}, we find that the width (or the depth for a cylindrical geometry) of the jet is $\sim 0.8''$, or 0.0056 pc. If we assume a flow velocity of 200 km s^{-1}, as did Meaburn et al. (2005), the mass loss rate would be $\sim 1.2 \times 10^{-7}$ $M_\odot$ yr^{-1}. It ought to be noted that when the disk-jet systems are exposed to photoionizing environments, the jet production is probably no longer a dominant role of mass loss from the circumstellar disk. Photoionization and dissipation of the disk then takes place, or at least consumes the circumstellar materials at a comparable rate as the mass ejection in the form of a jet. If we assume that evaporated flows associated with the dissipating disk of the jet source govern a comparably effective mass erosion as those of the proplyds in the Orion Nebula (Henney & O'Dell 1999), then for a mean mass loss rate of 4.1 x 10^{-7} $M_\odot$ yr^{-1} (Henney & O'Dell 1999) and a disk mass of 0.006 $M_\odot$ associated with the Rosette HH1 source (Li & Rector 2004), the estimated photodissipation

timescale of the relic disk is $\sim 10^4$ yrs. Given the more extreme environment the Rosette HH1 source faces, a mass loss rate an order of magnitude higher may be more likely and the disk dissipation time would be reduced to $\sim 10^3$ yrs.

6. Variability of the Jet-Driving Source

Photometric results of the jet driving source are presented in Figure 6, which shows irregular variations around the mean with an amplitude as large as ∼0.2 mag in the R band. This amplitude of variation is about one magnitude lower than that detected for the energy source of the Rosette HH2 jet, which amounts to as large as 1.4 mag in R (Li, Chu, & Gruendl 2007). Variations in the R band are primarily attributed to erratic fluctuations of the Hα emission of the source, which relies on a time-variable mass accretion rate, disk inhomogeneity, or otherwise chromospheric activity of the central YSO. The Rosette HH1 source's low amplitude of variation is believed to be due to a lack of circumstellar material and subsequently a subtle mass accretion rate, as shown by the nearly absent Hα emission from the jet source, although the irregular variation itself is consistent with a young status of evolution of the central source. We thus suggest that the Rosette HH1 source may well represent a transient phase of YSOs evolving rapidly from a CTTS to a WTTS by fast photodissipation of their circumstellar disks. Based on the time series photometric data achieved, we find no evidence of a binary origin of the jet source, which otherwise could imply a different mechanism of jet production. As noted in Section 2.3, the B band observations do not give very good results, although reminiscent irregular variations with a comparable magnitude of up to ∼0.25 mag are indeed indicated.

The spectral monitoring observations are not very useful for the Hα line profile because of the difficulty in background nebular subtraction, as discussed in Section 4. Nevertheless, the overall spectral characteristics of the star can be determined. We find that the spectral type appears to vary between F8V and F9V during the period of observations. This spectral change may be related to photo-erosion of the rotational disk with an inhomogeneous configuration.

7. Evidence for Fast Disk Dissipation and a Young Stellar Age?

Being immersed in the fierce UV radiation field of the Rosette, the optical jets associated with YSOs indicate either a jet production timescale of as long as 1-2 Myr, comparable to the evolutionary age of the main cluster NGC 2244, or that the YSOs have a much younger

age and the cocoons associated with their protostars had, in some way, been successfully shielded from the strong ionization fields.

Li (2005) investigated the YSOs with near infrared excesses, an indicator of the existence of circumstellar disks, of the young open cluster NGC 2244 based on the 2MASS database. The jet-driving sources in the Rosette, however, show infrared colors commensurate with those of WTTSs, which have spectral energy distributions indistinguishable from main-sequence dwarfs. See the color-color and color-magnitude diagrams in Figures 4 and 7 of Li (2005). This, along with the fact that none of the Rosette jet sources and their only rivals found near σ Orionis were detected by IRAS, suggests a lack of circumstellar material as compared to conventional YSOs driving outflows. This is in agreement with the estimated mass of 0.006 $M_{\odot}$ for the relic disk associated with the Rosette HH1 source (Li & Rector 2004), far below the typical value of $\sim$0.1 $M_{\odot}$ around CTTS. Given the emerging nature of the young open cluster with a turnoff age of 1.9 Myr (Park & Sung 2002), fast disk dissipation is suggested. Li & Rector (2004) suggest that this provides indirect observational evidence for the formation of isolated BDs and free-floating giant planets, as discovered in Orion by Zapatero Osorio et al. (2000), by UV dissipation of unshielded protostellar systems. This can be very important to our understanding of the formation of such sub-stellar and planetary mass objects, particularly in regions of massive star formation. Such UV dissipation could, on the other hand, impose strong effects on the formation of and hence the search for extra-solar planets around low-mass stars, the circumstellar disks of which could otherwise be potential sites of terrestrial planet formation. This alternatively introduces a viable solution to the long puzzle of how WTTS were formed as a consequence of fast CTTS evolution and the rapid dissipation of circumstellar disks under particular forming conditions near massive OB stars or in cluster environments.

The spatial distribution of the extreme jets with respect to the dozens of exciting OB stars of the spectacular H II region is presented in Figure 7, superimposed on which is the relic shell structure as delineated by the apparent congregation of excessive emission sources in the near infrared (Li 2005). This suggests the existence of a former working interface layer of the H II region with its ambient molecular clouds. The projected location of the energy source of the Rosette HH1 jet near the relic arc provides evidence of a triggered origin of its formation in or near the swept-up layer. The Rosette HH2 source has a similar radial distance from the statistical center of NGC 2244 (Li 2005) and introduces a similar origin. In this scenario, the jet sources should have a much younger age than the main cluster NGC 2244. Molecular gas and dust in the shell could have played an important role in shielding new generation protostellar objects from the harsh UV evaporation and ionization from the massive OB stars. It is therefore reasonable to infer that the jet sources have been directly exposed to the harsh photoionization fields recently.

8. Large-Scale High-Excitation Structures in the Rosette Nebula

Meaburn & Walsh (1986) first noted the existence of ionized knots and filaments in the southeastern quadrant of the Rosette's central cavity. The Rosette HH jets are also located in this region. All are prominent features in narrowband [O III] images, indicating a high excitation. Among these, knot C shows high-velocity components and is in association with a high excitation bow-shock at its tip (Clayton & Meaburn 1995; Clayton et al. 1998). This feature is believed to be a HH flow, though no apparent energy source has yet been identified.

However, a giant shock-like structure to the west of the Rosette HH1 jet can be easily identified (Figure 8). At a distance of ∼1.5 kpc, its large-scale appearance and lack of a potential exciting source seem to exclude the possibility of a Herbig-Haro origin. The preferential distribution of these high-excitation structures to the southeast edge of the H II region suggests a possible association with the large Monoceros Loop supernova remnant (SNR) projected to the northeast of the Rosette Nebula. While there is no morphological evidence for dynamical interactions between these two objects, it is possible that some of the high-excitation structures in the Rosette Nebula are caused by the Monoceros Loop SNR's ballistic ejecta that proceeds ahead of the SNR shock front. To test this scenario, proper motion or abundance measurements of the high-excitation structures in the Rosette Nebula are needed.

Alternatively, we propose that these structures are globules or former dust pillars, similar to those around the working surface of the H II region, that have been overrun by the ionization front and are now in the process of photodissipation, as is the fate of the HH jets in this region. At least one high-excitation structure is likely associated with a neutral cometary knot (see Figure 8), the tip of which is highly ionized and has an appearance resembling those in the Orion Nebula (Bally et al. 2000), but with a physical size roughly 4 times larger.

9. Summary

We present follow-up high-qaulity imaging and echelle spectroscopic observations of the Rosette HH1 jet. The high angular and spectral resolution allow us to determine accurately the contributions from the H II region, jet, and star. The expansion of the H II region and the kinematics of the jet are consistent with the previous measurements by Meaburn et al. (2005). Using the [S II] doublet ratios, we further determined the electron density of the jet, ∼1000 cm^{-3}.

With a careful subtraction of the nebular and jet components, we find the stellar Hα line

is dominated by a broad absorption profile with little or no emission component, indicating a lack of substantial circumstellar material. The circumstellar material has most likely been photo-evaporated by the strong UV radiation field in the Rosette Nebula. The evaporation time scale is 10^3 – 10^4 yr. The Rosette HH1 jet source provides evidence for an accelerated evolution from a CTTS to a WTTS due to the strong UV radiation field; therefore, both CTTSs and WTTSs can be spatially mixed in regions with massive star formation.

Finally, we suggest that the giant high-excitation structures residing at the center of the Rosette Nebula may be globules or former dust pillars in the midst of UV dissipation. Further observations of the nebular kinematics are needed to determine whether these are dissipating interstellar structures or related to the supernova ejecta associated with the Monoceros Loop SNR.

We greatly appreciate the helpful comments and suggestions from the referee of the paper, John Meaburn. Thanks to the team working with the Hsing-Hua 80cm telescope for their help on coordinating the photometric observations. This project is supported by the National Natural Science Foundation of China through grant No.10503006.

REFERENCES

Andrews, S. M., Reipurth, B., Bally, J., & Heathcote, S. R. 2004, ApJ, 606, 353

Bally, J., O'Dell, C. R., & McCaughrean, M. J. 2000, AJ, 119, 2919

Bally, J. & Reipurth, B. 2001, ApJ, 546, 299

Bally, J., Sutherland, R. S., Devine, D., & Johnstone, D. 1998, AJ, 116, 293

Clayton, C. A., & Meaburn, J. 1995, A&A, 302, 202

Clayton, C. A., Meaburn, J., Lopez, J. A., & Christopoulou, P. E., & Goudis, C. D. 1998, A&A, 334, 264

Dorland, H., & Montmerle, T. 1987, A&A, 177, 243

Henney, W. J., & O'Dell, C. R. 1999, AJ, 118, 2350

Hensberge, H., Pavlovski, K., & Verschueren, W., 2000, A&A, 358, 553

Johnstone, D., Hollenbach, D., & Bally, J. 1998, ApJ, 499, 758

Li, J. Z. 2003, Chinese J. Astron. Astrophys., 3, 495

Li, J. Z. 2005, ApJ, 625, 242

Li, J. Z., Chu, Y.-H., & Gruendl, R. A. 2007, AJ, submitted

Li, J. Z., & Rector, T. A. 2004, ApJ, 600, L67

Looney, L. W., Tobin, J. J., & Fields, B. D. 2006, ApJ, 652,1755 (astro-ph/0608411)

Maíz-Apellániz, J., Walborn, N. R., Galué, H. Á., & Wei, L. H. 2004, ApJS, 151, 103

Massey, P., Strobel, K., Barnes, J. V., & Anderson, E. 1988, ApJ, 328, 315

Meaburn, J., Lopez, J. A., Richer, M. G., Riesgo, H., & Dyson, J. E. 2005, AJ, 130, 730

Meaburn, J., & Walsh, J. R. 1996, MNRAS, 220, 745

Osterbrock, D. E. 1989, Astrophysics of Gaseous Nebulae and Active Galactic Nuclei (Mill Valley: University Science Books)

Panagia, N. 1973, AJ, 78, 929

Park, B.-G., & Sung, H. 2002, AJ, 123, 892

Pérez, M. R., Thé, P. S., & Westerlund, B. E. 1987, PASP, 99, 1050

Reipurth, B., Bally, J., Fesen, R. A., & Devine D. 1998, Nature, 396, 343

Townsley, L. K., Feigelson, E. D., Montmerle, T., Broos, P. S., Chu, Y.-H., & Garmire, G. P. 2003, ApJ, 593, 874

Welsh, B. Y., Sfeir, D. M., Sallman, S., & Lallement, R. 2001, A&A, 372, 516

Whitworth, A. P., & Zinnecker, H. 2004, A&A, 427, 299

Zapatero Osorio, M. R., Bejar, V. J. S., Martin, E. L., Rebolo, R., Barrado y Navascués, D., Bailer-Jones, C. A. L., & Munct, R. 2000, Science, 290, 103

Fig. 1.— Hα image of the Rosette HH1 jet obtained with the KPNO 4 m telescope. North is up, and east is to the left.

Fig. 2.— Echelle spectrograms of the Rosette HH1 jet. Single-order echelle spectrograms of the jet system covering only the Hα and [N II] λ6583 lines are presented in the left panels. The continuum emission at $Y = 0''$ of each spectrogram is from the jet-driving source. The multi-order observations of the [N II] λ6583, [S II] λ6731 and [O III] λ5007 lines are shown in the right panels.

Fig. 3.— Line profiles of Hα (left panel) and [N II] λ6583 (right panel) extracted at positions across the stellar spectrum, using $1''$ windows and $0''.5$ steps. These profiles show contributions from the stellar continuum, jet emission, and background nebular emission.

Fig. 4.— Nebula-subtracted stellar spectra around Hα (left panel) and [N II] λ6583 (right panel, serving as a quality control of the nebula subtraction). Note the narrow, blue-shifted emission component and the broad, red-shifted absorption associated with Hα.

Fig. 5.— The net stellar spectrum with a larger wavelength coverage. Top panel: nebula-subtracted stellar spectrum. Middle panel: the clean jet spectrum after background subtraction. Bottom panel: net stellar spectrum after the removal of both the nebular background and the jet contribution.

Fig. 6.— Photometric variations of the jet source in the R band. Note the irregular variations at low amplitudes, which are detected on timescales of minutes to hours around a fitted mean level (dot-dashed line).

Fig. 7.— Spatial distribution of the Rosette jets with respect to the ionizing massive OB stars that excavated the H II region (Townsley et al. 2003). The spectral types of the OB stars are also marked on the DSS (Digital Sky Survey) R band image of Rosette.

Fig. 8.— Large high-excitation shock structures in the Rosette Nebula. Note the presence of at least one cometary knot among these seemingly inter-related structures. The tip of the neutral knot is clearly highly ionized and has an appearance resembling those identified in the Orion Nebula (Bally et al. 2000), but $\sim$4 times larger.

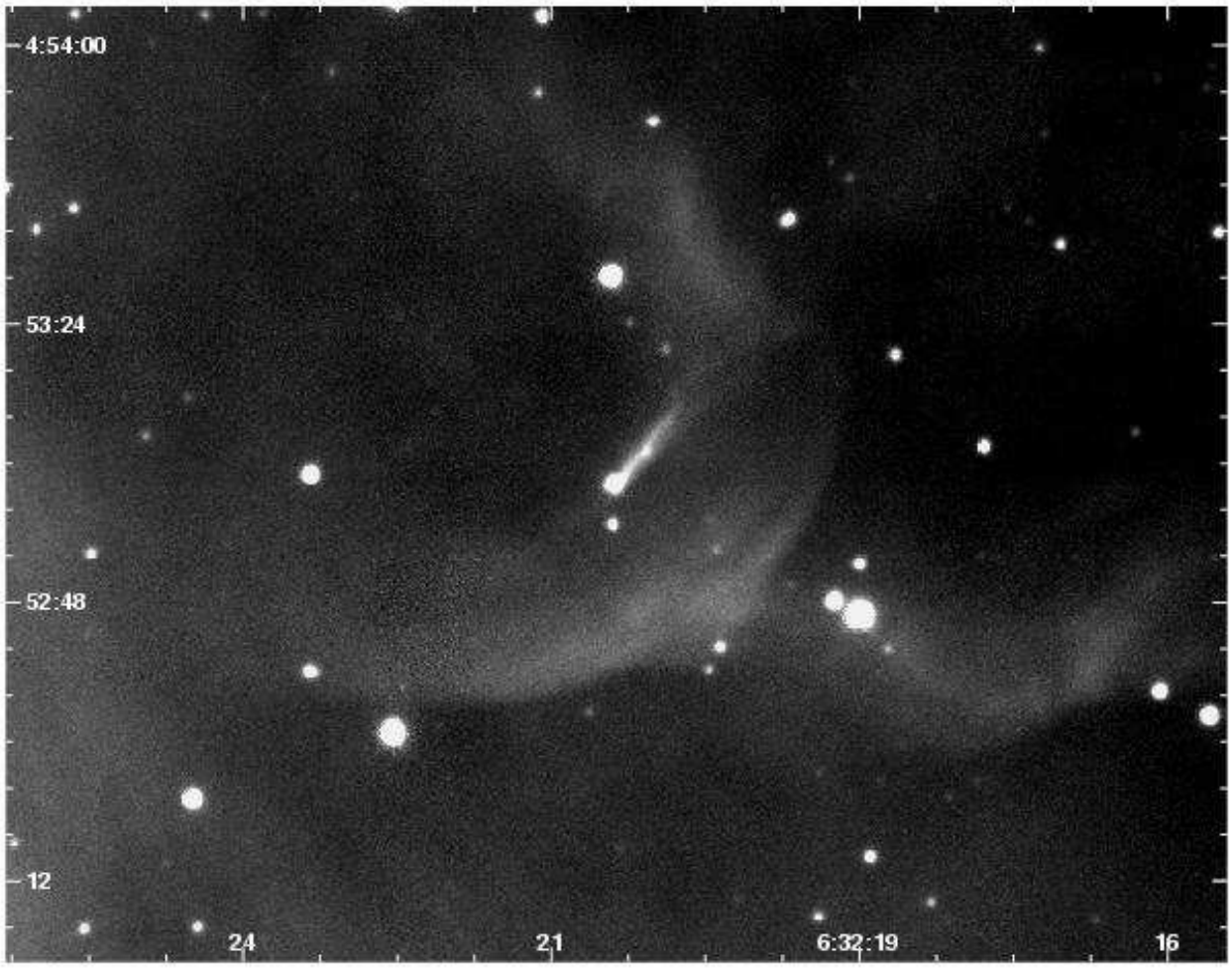

f1.ps

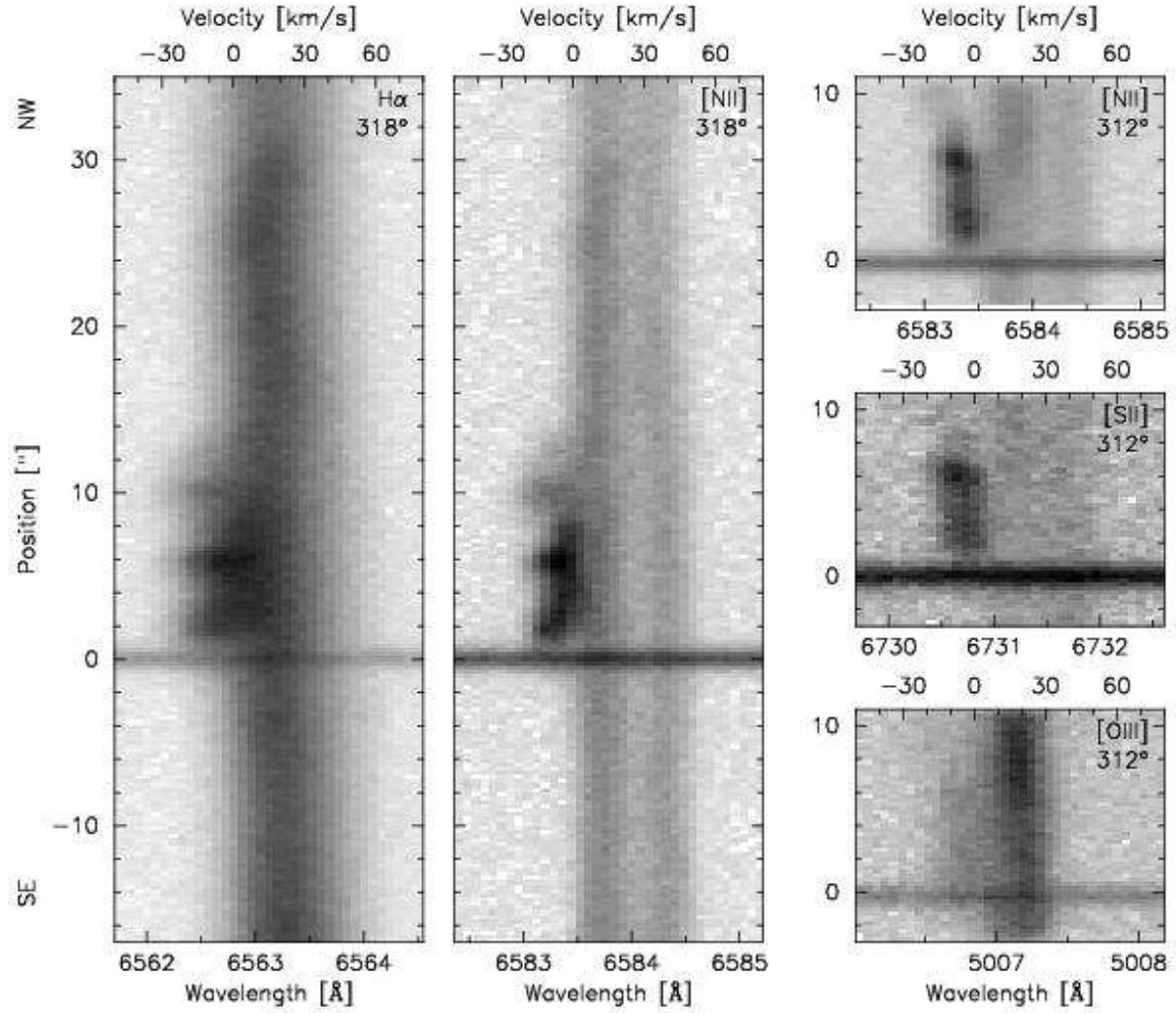
Velocity [km/s]
−30 0 30 60
Hα
318°
[NII]
318°
[NII]
312°
[SII]
312°
[OIII]
312°
NW
SE
Position ["]
30
20
10
0
−10
6562 6563 6564
6583 6584 6585
6730 6731 6732
5007 5008
Wavelength [Å]

f2.ps

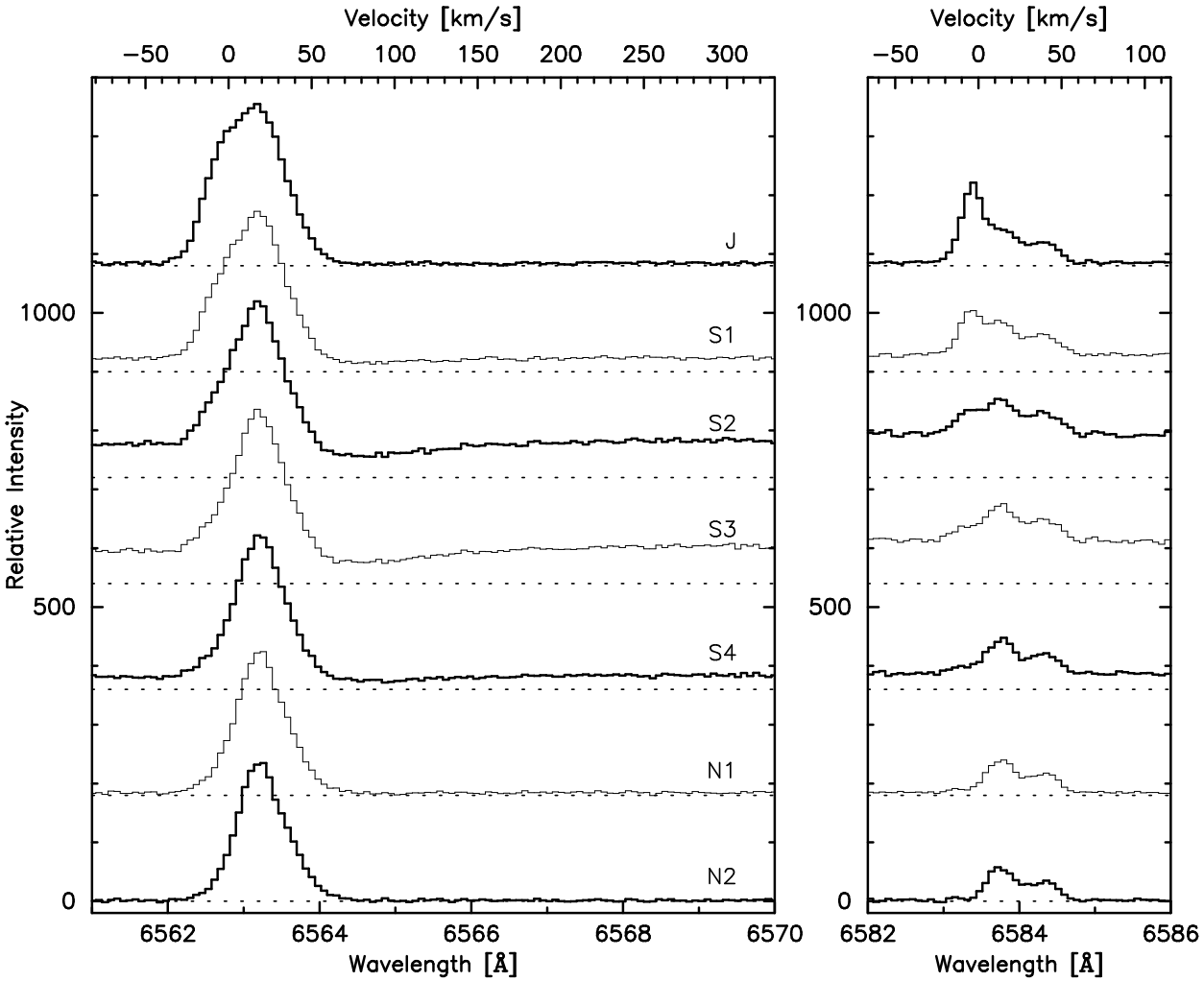
Velocity [km/s]
−50
0
50
100
150
200
250
300
J
S1
S2
S3
S4
N1
N2
1000
500
0
Relative Intensity
6562
6564
6566
6568
6570
Wavelength [Å]
Velocity [km/s]
−50
0
50
100
1000
500
0
6582
6584
6586
Wavelength [Å]

f3.ps

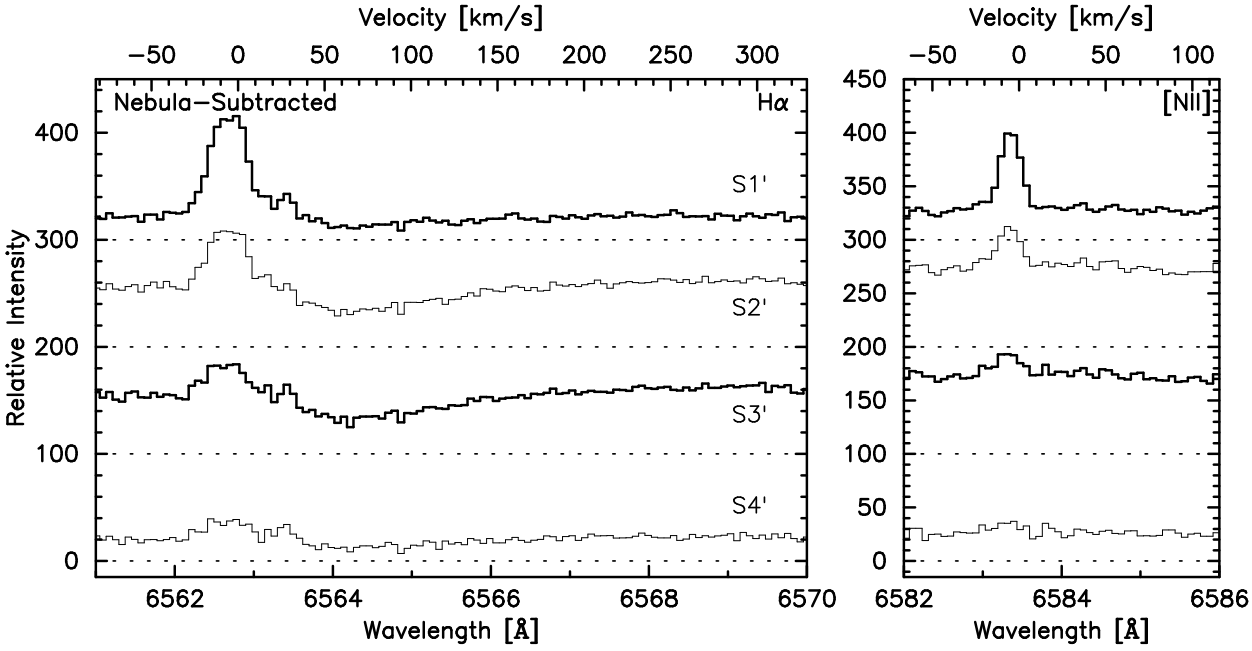
Velocity [km/s]
−50
0
50
100
150
200
250
300
Nebula−Subtracted
Hα
S1'
S2'
S3'
S4'
Relative Intensity
400
300
200
100
0
6562
6564
6566
6568
6570
Wavelength [Å]
Velocity [km/s]
−50
0
50
100
[NII]
450
400
350
300
250
200
150
100
50
0
6582
6584
6586
Wavelength [Å]

f4.ps

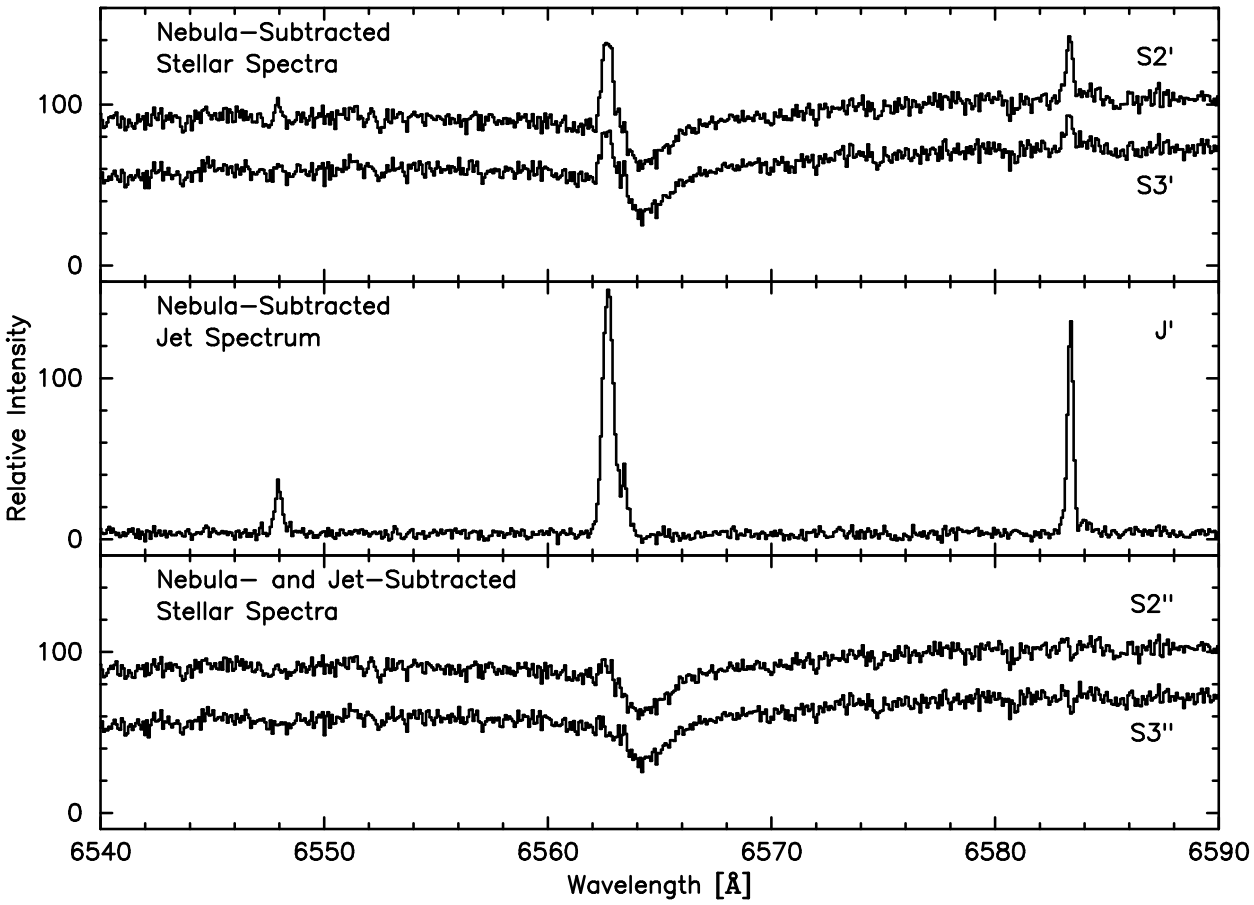
Nebula–Subtracted
Stellar Spectra
S2'
S3'
Nebula–Subtracted
Jet Spectrum
J'
Nebula– and Jet–Subtracted
Stellar Spectra
S2''
S3''
Relative Intensity
100
0
6540
6550
6560
6570
6580
6590
Wavelength [Å]

f5.ps

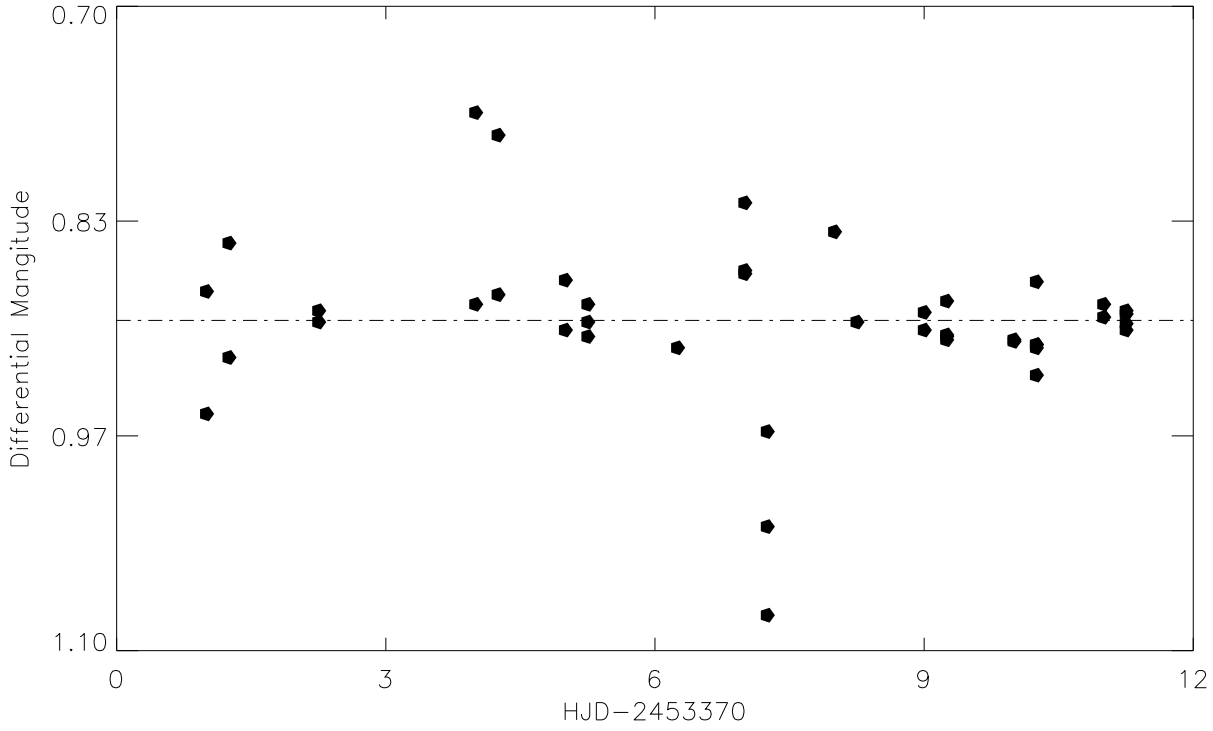

f6.ps

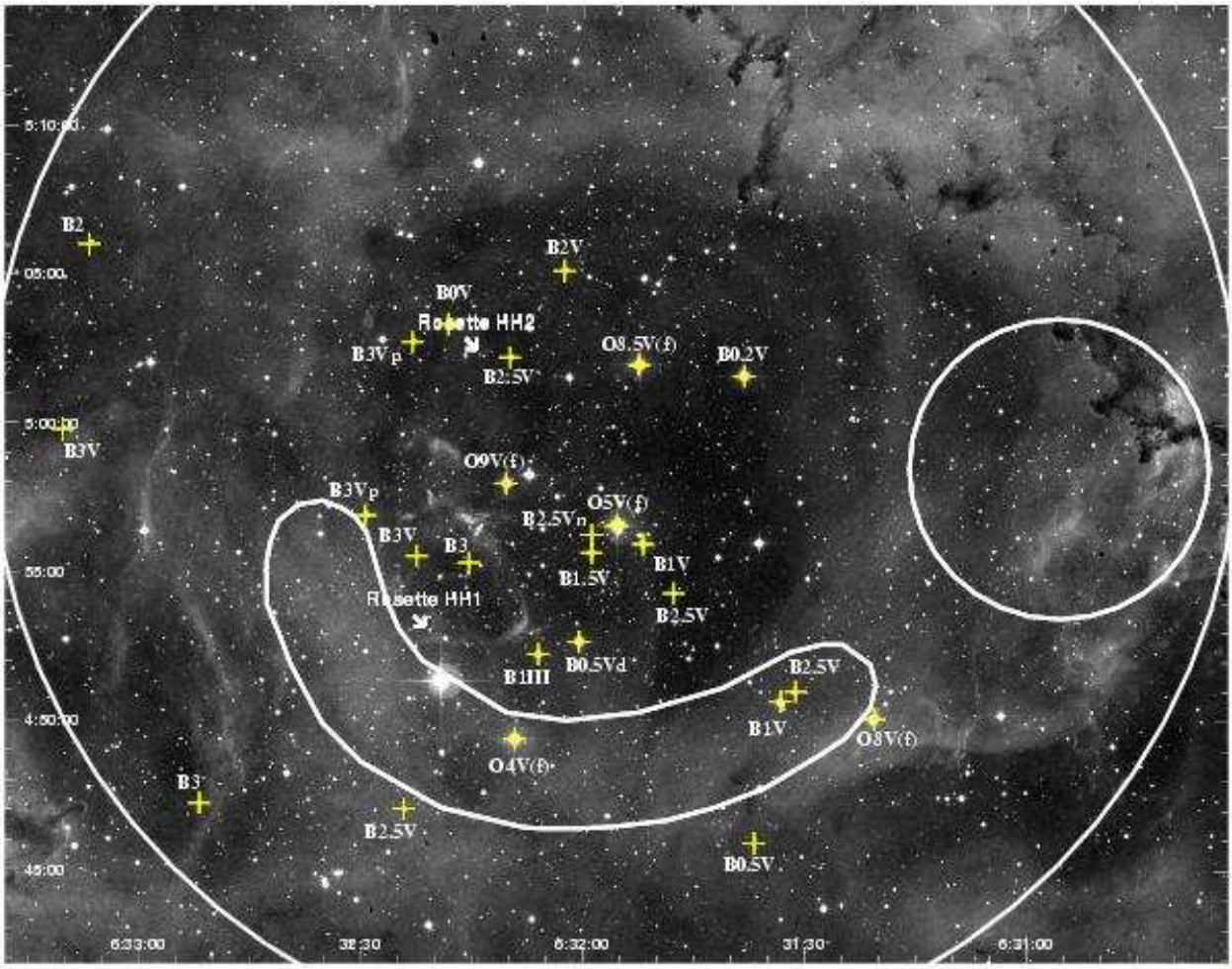
B2
B2V
B0V
Rosette HH2
B3Vp
B2.5V
O8.5V(f)
B0.2V
B3V
O9V(f)
B3Vp
O5V(f)
B2.5Vn
B3V
B3
B1V
B1.5V
Rosette HH1
B2.5V
B1III
B0.5Vd
B2.5V
B1V
O8V(f)
O4V(f)
B3
B2.5V
B0.5V
6:33:00
32:30
6:32:00
31:30
6:31:00

f7_color.ps

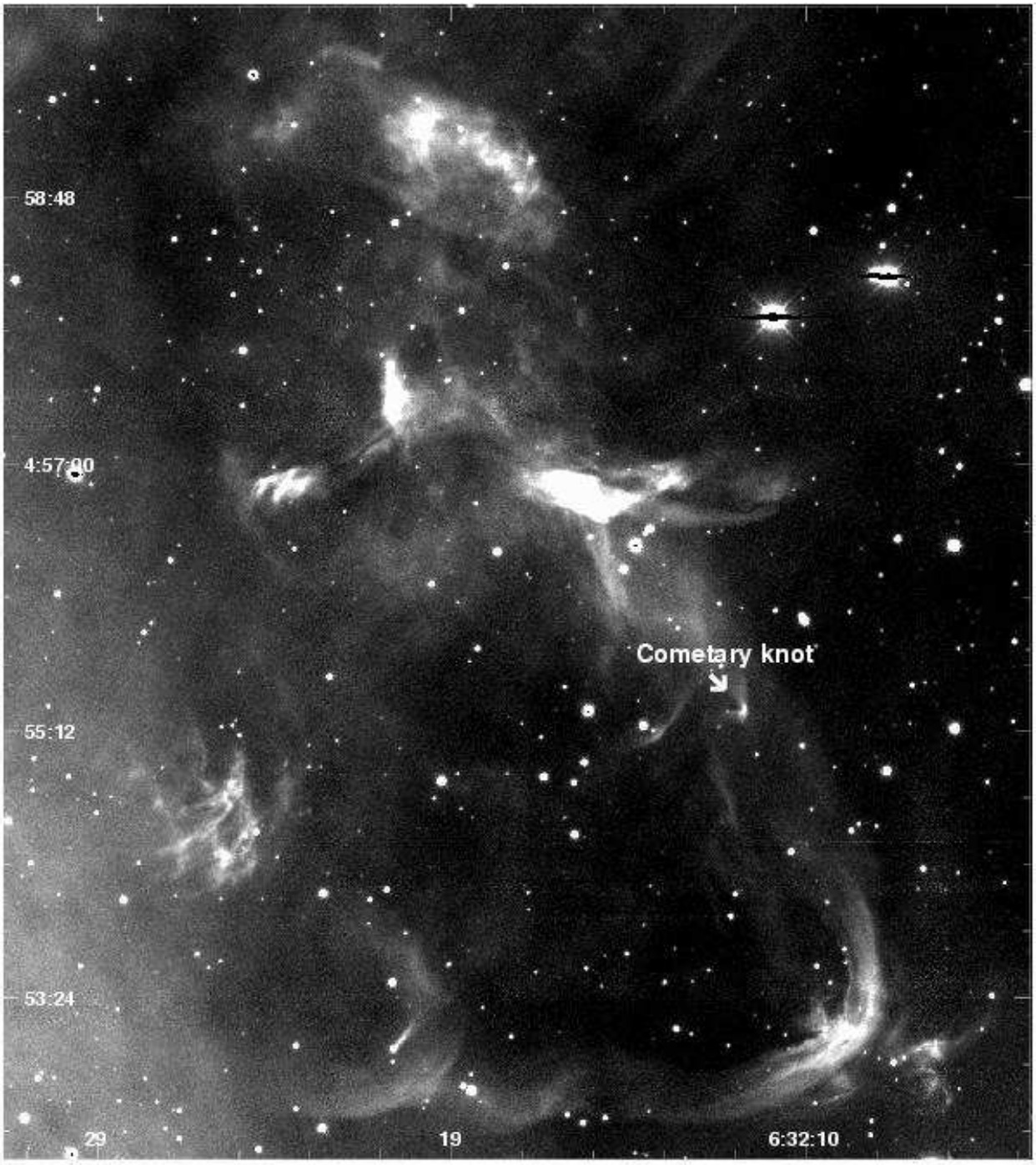

f8.ps